AMERICAN SOCIETY FOR MICROBIOLOGY | Applied and Environmental Microbiology®

ENVIRONMENTAL MICROBIOLOGY

Microbial Community Dynamics during a Harmful *Chrysochromulina leadbeateri* Bloom in Northern Norway

Nerea J. Aalto,[a,b] Hannah Schweitzer,[a,b] Erlend Grann-Meyer,[a] Stina Krsmanovic,[a] Jon B. Svenning,[a] Lars Dalheim,[a] Sebastian Petters,[a] Richard A. Ingebrigtsen,[a] Chris J. Hulatt,[c] Hans C. Bernstein[a,b]

[a]Norwegian College of Fisheries Sciences, UiT–The Arctic University of Norway, Tromsø, Norway
[b]The Arctic Centre for Sustainable Energy, UiT–The Arctic University of Norway, Tromsø, Norway
[c]Faculty of Biosciences and Aquaculture, Nord University, Bodø, Norway

ABSTRACT A harmful algal bloom occurred in late spring 2019 across multiple, interconnected fjords and bays in northern Norway. The event was caused by the haptophyte *Chrysochromulina leadbeateri* and led to severe fish mortality at several salmon aquaculture facilities. This study reports on the spatial and temporal succession dynamics of the holistic marine microbiome associated with this bloom by relating all detectable 18S and 16S rRNA gene amplicon sequence variants to the relative abundance of the *C. leadbeateri* focal taxon. A k-medoid clustering enabled inferences on how the causative focal taxon cobloomed with diverse groups of bacteria and microeukaryotes. These coblooming patterns showed high temporal variability and were distinct between two geographically separated time series stations during the regional harmful algal bloom. The distinct blooming patterns observed with respect to each station were poorly connected to environmental conditions, suggesting that other factors, such as biological interactions, may be at least as important in shaping the dynamics of this type of harmful algal bloom. A deeper understanding of microbiome succession patterns during these rare but destructive events will help guide future efforts to forecast deviations from the natural bloom cycles of the northern Norwegian coastal marine ecosystems that are home to intensive aquaculture activities.

IMPORTANCE The 2019 *Chrysochromulina leadbeateri* bloom in northern Norway had a major impact on the local economy and society through its devastating effect on the aquaculture industry. However, many fail to remember that *C. leadbeateri* is, in fact, a common member of the seasonal marine microbiome and the same spring phytoplankton blooms that support the marine ecosystem. It is challenging to draw any conclusions about exact causation behind the harmful bloom of 2019, especially since the natural bloom cycles of *C. leadbeateri* are not well understood. This study begins to fill major knowledge gaps that may lead to future forecasting abilities, by providing a molecular-based investigation of the destructive 2019 bloom that presents new insights into a seasonal marine microbial ecosystem during one of these sporadically reoccurring events.

KEYWORDS marine microbiome, harmful algae, aquaculture, Norway, harmful algal bloom, succession, time series, Troms, rRNA

Harmful algal blooms (HABs) are common in warm and temperate waters but also occur in northern cold-water ecosystems (1, 2). These blooms pose a serious risk for aquaculture activities, because farmed fish cannot escape from developing adverse conditions caused by marine microalgae. Previously, the most infamous northern Norwegian bloom occurred in 1991 in Ofotfjord, causing high mortality in affected fish farms (3). Smaller HAB incidents have occurred since then, although they have gained little attention in mainstream media (4). The salmon aquaculture industry has expanded over the past decades to a landing value of salmon that reached 7 billion U.S. dollars (USD) in

Editor Laura Villanueva, Koninklijk Nederlands Instituut voor Onderzoek der Zee

Address correspondence to Hans C. Bernstein, Hans.C.Bernstein@uit.no.

The authors declare no conflict of interest.

Received 9 November 2022
Accepted 9 December 2022
Published 9 January 2023

2019 (5). Therefore, the Norwegian economy and seafood export supply was seriously threatened when a deadly HAB of *Chrysochromulina leadbeateri* (haptophyte) reoccurred and caused massive fish mortalities in the Troms and Nordland regions of coastal northern Norway from mid-May to the beginning of June 2019 (6). The fish loss was ca. 14,500 metric tonnes, which is the highest amount among fish kill-related HABs in Scandinavia since 1988 (2, 6). Knowledge that can eventually inform causation is very limited, especially in the context of seasonal microbial blooming dynamics, detailed taxonomy of coblooming species, and the environmental conditions during the 2019 incident.

Marine HABs are often associated with altered inorganic nitrogen-to-phosphate (N:P) ratios in the surface water, coupled with a long period of high irradiance, calm weather, and strong surface water stratification (7–9). However, the physical environment is not the only determining factor for the strength and duration of a HAB (10), as more evidence is showing that biological interactions impact microalgal bloom dynamics. The roles and importance of coblooming members of the marine microbiota are becoming more recognized factors in structuring the temporal and spatial relationships of phytoplankton communities (e.g., 11–13). Therefore, it is important to observe and catalogue the blooming patterns of the whole surface water microbiome while studying the ecology of focal taxa involved with HAB events.

The spring-summer phytoplankton seasonal succession along the coast of northern Norway has been extensively studied, but the majority of data collected to date have used only morphology-based identification of microalgal taxa, which limited the resolution of taxonomic diversity of these blooming patterns (e.g., 14–17). From previous studies, we know that the onset of the spring bloom occurs in late March/early April, and it is driven by increased irradiance as the region undergoes a shift from polar night to spring, within elevated winter nutrient concentrations and a well-mixed water column (15, 18, 19). These conditions lead to a rapid and intense increase of many chain-forming centric diatoms that cobloom with *Phaeocystis pouchetii* (haptophyte), which often outlasts the diatoms and persists throughout the summer (14, 18). The spatial and interannual variation of the late bloom (May to June) phytoplankton community can comprise a diverse mix of low-nutrient-tolerant, heterotrophic, and mixotrophic species belonging to dinoflagellates, cryptophytes, ciliates, and other small flagellates (15, 16). The roles and taxonomic succession patterns of bacterioplankton in these annual blooms are essentially unknown for the region.

Time series analysis combined with high-resolution taxonomic screening such as 16S and 18S rRNA gene amplicon sequencing is an important method for evaluating microbial succession dynamics and the ecological factors that drive blooms (11, 20). However, knowledge about the nature of taxon-specific and -nonspecific blooming patterns is poor because identification of these hidden dynamics is challenging. Therefore, information obtained from time series analysis relies strongly on sampling resolution and length of time series, as previous high-frequency time series studies have revealed rapid turnover (days) within abundances of marine microbial community members (11, 12). In addition, analytical approaches play a central role as tools to assess communities with covarying succession dynamics and, further, to infer potential microbial interactions and responses on changes in environmental conditions which are key aspects for understanding the development of HAB (11, 21). For example, clustering algorithms such as k-medoid allow us to parse complex communities into smaller groups of taxa which share similar temporal dynamics and thus may help to identify the key taxa driving the observed cooccurrence (21).

Our aim was to contribute to the knowledge of the ecology and microbial succession dynamics associated with the *C. leadbeateri* HAB, whose role as a causative agent for this devastating event has already been established (6, 22). This was accomplished by asking three targeted research questions. (i) How did the marine microbiome composition change during the 2019 HAB event in relation to the focal taxon (*C. leadbeateri*)? (ii) What were the major blooming (temporal) patterns among prokaryotes and microeukaryotes and which taxa cobloomed with the focal taxon? (iii) Which environmental factors were associated with the observable differences in the marine microbiome composition? This

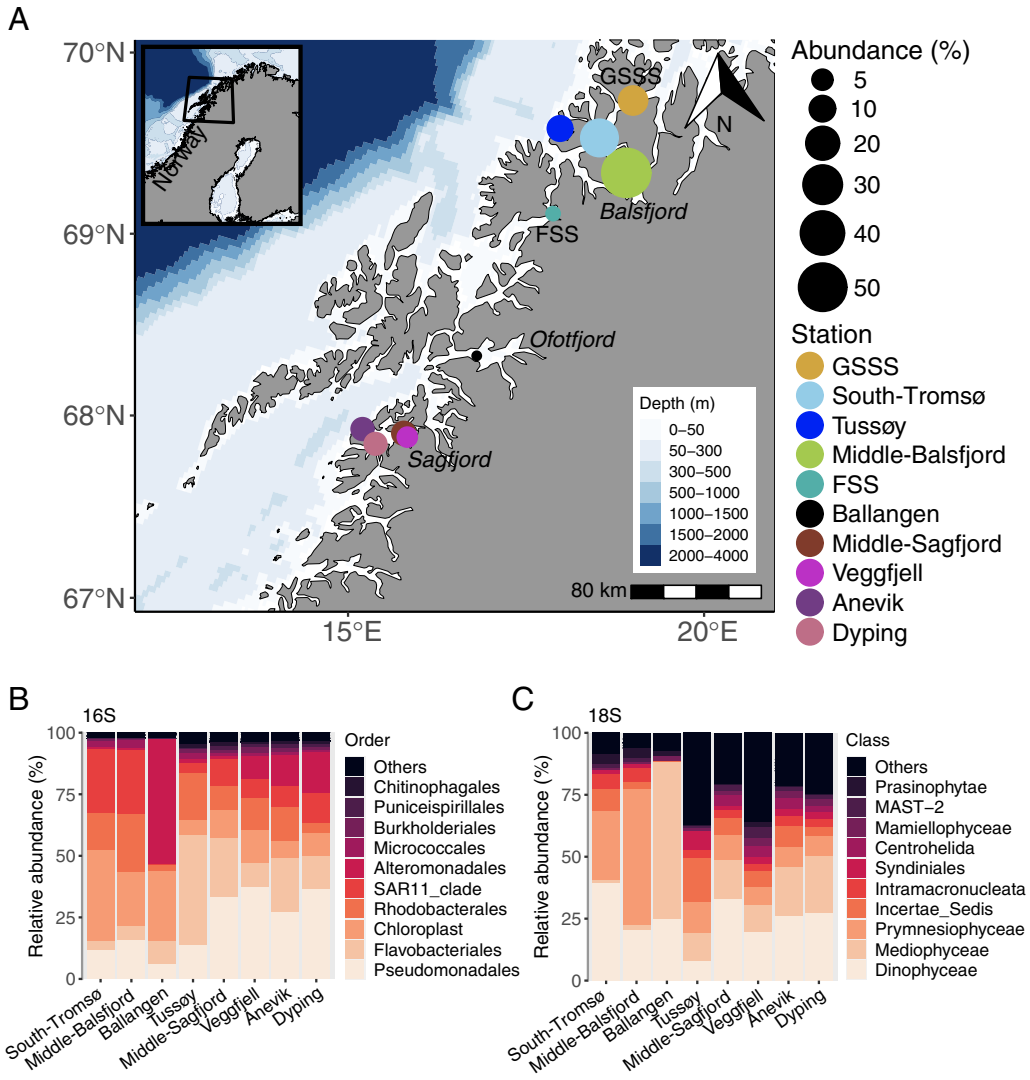

FIG 1 A map showing the geographical area in northern Norway where a *Chrysochromulina leadbeateri*-related harmful algal bloom occurred in summer 2019. The main sample locations are named on the map. (A) Microbial DNA for 18S rRNA and 16S rRNA amplicon sequence analysis was collected once from the marked stations, except for FSS (Finnfjord sampling station) and GSSS (Grøtsund sampling station), which are the primary stations of this time series study and were sampled 7 and 8 times, respectively, between May 27 and June 21. The sizes of the circles represent the relative abundance of the *C. leadbeateri* focal taxon (average relative abundance for FSS and GSSS stations across all samples). Not all of the stations represent localities where HAB-related fish mortality was experienced. (B and C) Taxonomic composition of the most abundant (B) prokaryotes (16S) and (C) microeukaryotes (18S) retrieved from amplicon sequence variant (ASV) tables specified at the order and class taxonomic rank level, respectively. Note that the FSS and GSSS stations are excluded from panels B and C as the taxonomic composition across time series is shown in Fig. 2.

study provides a molecular-based investigation of the destructive 2019 *C. leadbeateri* HAB and presents new insights into a seasonal marine microbial ecosystem that can have a major impact on the social-economic welfare of Norway through its relation to the aquaculture industry.

RESULTS

Geographical distribution of the focal taxon in relation to fish mortality. We detected the *Chrysochromulina leadbeateri* focal taxon (class *Prymnesiophyceae*) in various relative abundances across the bloom-affected region of the northern Norwegian coast and fjords (Fig. 1A). These data are in concordance with other investigations of this 2019 HAB event that established *C. leadbeateri* as a causative agent of fish

mortality (6, 22). Its abundance varied between 0.4 and 51.8% of the microeukaryotic (phytoplankton and heterotrophic protist) community assessed via 18S amplicon sequencing through the HAB-affected region. The highest relative abundances of the focal taxon, *C. leadbeateri*, recorded in our molecular sampling campaign were obtained in the northern portion of the HAB-affected region, which included Middle-Balsfjord, South-Tromsø, and Tussøya stations, and the Grøtsund sampling station (GSSS) (Fig. 1A). The microbial community composition within a taxonomic rank level class for microeukaryotes and order for prokaryotes was relatively similar between the Middle-Balsfjord, South-Tromsø, and GSSS stations with increased relative abundance of 18S amplicon sequence variants (ASVs) and 16S ASVs indicative of dinoflagellates (class *Dinophyceae*) and the order *Flavobacteriales*, respectively, toward station GSSS (Fig. 1B and C). The relative abundance of ASVs belonging to the focal taxon were low in Ballangen (Ofotfjord), where the HAB was first reported to originate with high fish mortality in mid-May (6). The community structure from Ballangen was also distinct compared to other samples, as it was dominated by 18S ASVs indicative of centric diatoms, notably from the genus *Skeletonema* (class *Mediophyceae*), and 16S ASVs classified within the genera *Pseudoalteromonas* and *Colwellia* (order *Alteromonadales*) (Fig. 1B and C and genus level abundances in single-time-point stations in Data sets S2 and S3 in the supplemental material). The relative abundance of *C. leadbeateri* was higher in samples collected from the Sagfjord stations (Anevik, Dyping, Veggfjell, and Middle-Sagfjord), south of Ofotfjord, than in the Ballangen and Finnfjord sampling station (FSS) stations (Fig. 1A). The microeukaryotic community in the Sagfjord location was especially diverse, with multiple distinct groups of dinoflagellates and centric diatoms being the most abundant. In contrast to the other sampling locations, the 16S prokaryotic ASVs among the Sagfjord stations were predominantly comprised by the order *Pseudomonadales* (Fig. 1B and C).

Microbiome dynamics across the bloom. The microeukaryotic and prokaryotic community composition (i.e., beta diversity) changed across the time series sampling campaign at FSS (permutational multivariate analysis of variance [PERMANOVA]: 16S, $R^2 = 0.36$ and $P = 0.004$; 18S, $R^2 = 0.56$ and $P = 0.003$) and GSSS (PERMANOVA: 16S, $R^2 = 0.36$ and $P = 0.002$; 18S, $R^2 = 0.40$ and $P = 0.002$) by pairwise comparison of the first and last sample day within each data set. These dynamic communities were also significantly dissimilar between the two time series stations (PERMANOVA: 16S, $R^2 = 0.30$ and $P = 0.001$; 18S, $R^2 = 0.46$ and $P = 0.001$) (Table S3). GSSS showed higher species richness than FSS as measured by the number of observed ASVs per sample day; 235 to 288 and 244 to 358 ASVs for 16S and, accordingly, 306 to 415 and 161 to 265 ASVs for 18S in GSSS and FSS, respectively, although the difference was statistically significant only for the 18S data set (Tukey test, $P < 0.01$) (Fig. S6).

Among the most abundant microeukaryotes assigned to the taxonomic level class, only 18S ASVs indicative of *Cryptophyceae*, *Mediophyceae*, *Dinophyceae*, and *Prymensiophyceae* (including the focal taxon) were shared between both stations (Fig. 2A and B). The observed community in FSS was dominated by taxa classified as *Cryptophyceae* (9 to 49% of the relative abundance), comprising mainly ASVs assigned to the genus *Teleaulax*, that showed strong temporal variability in the second half of the time series (Fig. 2A and genus level abundances in FSS in Data set S4). The predominant taxon observed from GSSS was classified as *Dinophyceae*, which accounted for 34 to 54% of the relative abundance during the time series (Fig. 2B). Most of the ASVs belonging to the class *Dinophyceae* were not assigned to a lower taxonomic level.

A change in community structure was visually observed at both stations during the middle of the observed bloom; between days 7 and 15 in FSS and between days 11 and 16 at the GSSS station (Fig. 2A and B). This shift was observed with an increased relative abundance of ASVs indicative of centric diatoms (class *Mediophyceae*) in both stations and the class *Coscinodiscophytina* in FSS, which were almost exclusively represented by ASVs indicative of the genus *Leptocylindrus* (Fig. 2A and B and Data set S4). The class *Mediophyceae* comprised ASVs that were classified within different genera

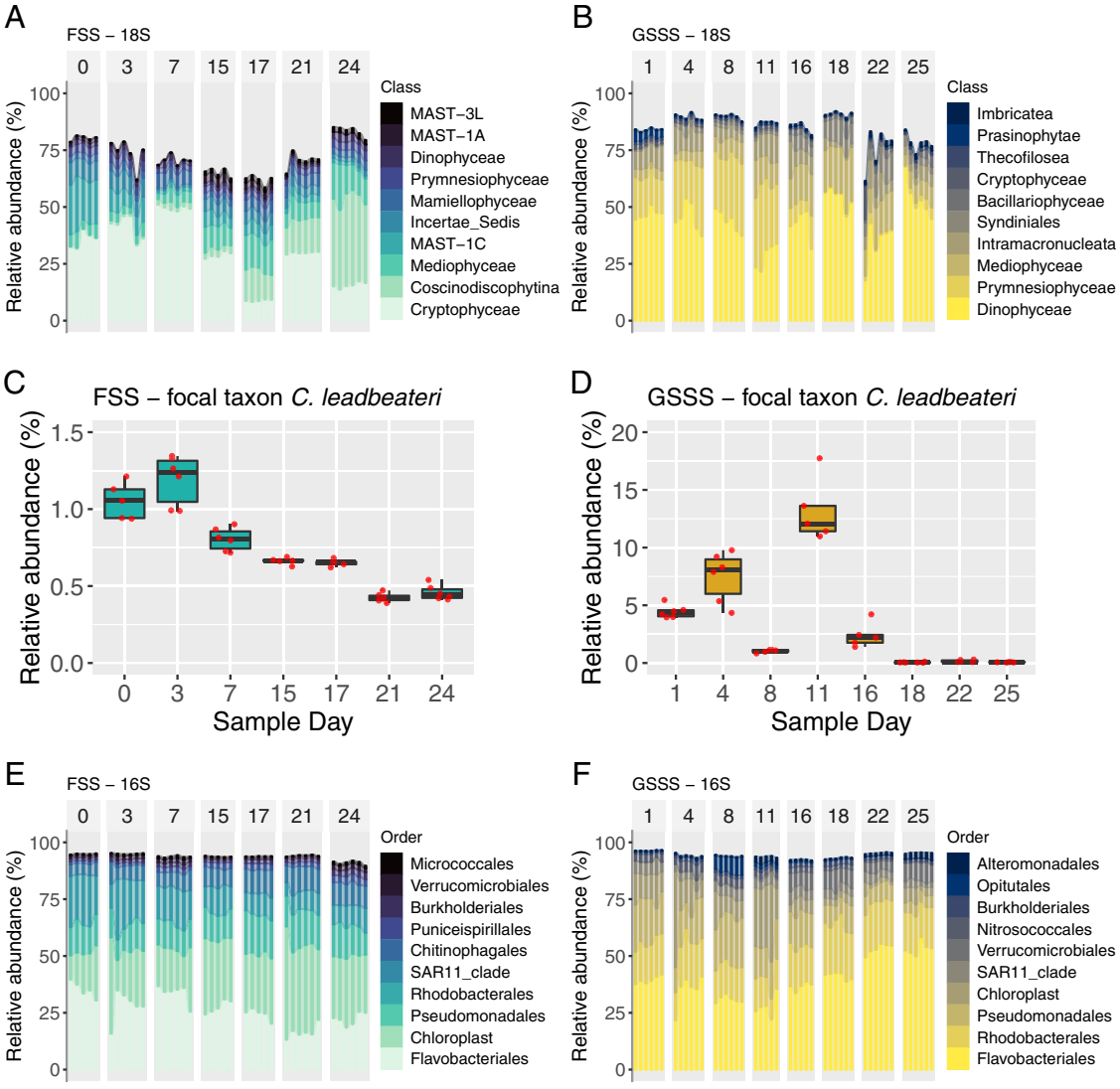

FIG 2 Comparative composition of the most common microeukaryotic and prokaryotic taxa collected from the time series sample stations and determined via 16S and 18S rRNA amplicon analysis. (A and B) Microeukaryotes classified at the class taxonomic rank level (A) in FSS and (B) in GSSS. (C and D) The temporal change in relative abundance of the *C. leadbeateri* focal taxon (C) in FSS and (D) in GSSS. (E and F) Prokaryotes classified at the order taxonomic rank level (E) in FSS and (F) in GSSS.

between stations, such as *Acrocellulus* at FSS and *Thalassiosira* at GSSS (Data sets S4 and S5). In FSS, the contribution of the class *Prymnesiophyceae* to the community composition was minor in comparison to GSSS (Fig. 2A and B) and was composed mainly of ASVs classified in the genus *Chrysochromulina* (2 to 3% of relative abundance) as classified by the SILVA v138.1 database (genus level abundances in FSS and GSSS Data set S4 to S5) but also ASVs assigned to the *Chrysochromulina* focal taxon (0.5 to 1% of relative abundance of genus OLI16029 within SILVA v138.1) (Fig. 2C) as verified by manual sequence alignment (Fig. S4). In GSSS, class *Prymnesiophyceae* prevailed until day 11 (42% of the relative abundance) and thereafter drastically decreased, while ASVs assigned to *Syndiniales* concurrently increased (Fig. 2B). The majority of those ASVs belonging to the class *Prymnesiophyceae* were assigned to the genera *Phaeocystis* and the focal taxon (*C. leadbeateri*) (genus level abundances in GSSS in Data set S5). The pronounced decrease in abundance of the focal taxon at day 8 coincided with highest relative abundance of *Phaeocystis* (Fig. 2D and Data set S5).

The 16S ASVs (classified at the order level) showed less temporal variability than the 18S ASVs (at the class level) across the time series in FSS and GSSS. The taxa with the

highest relative abundances were the same in the FSS and GSSS sample stations (Fig. 2E and F). Taxa classified to the order *Flavobacteriales* showed the highest relative abundance, with ASVs belonging *Rhodobacterales* and *Pseudomonadales* being common as well in both time series stations (Fig. 2E to F). The FSS and GSSS locations harbored distinctly different relative abundances of genera assigned to *Flavobacteriales*. At GSSS, the dominant genera were *Polaribacter*, *Ulvibacter*, *Formosa*, and the NS5 marine group, compared to FSS, where the NS5 and NS9 marine groups were dominant (Data sets S4 and S5). At GSSS, members of the order *Verrumicrobiales* increased in relative abundance (from 1 to 8%) within the same time frame that major changes in the microeukaryotes were observed (Fig. 2F). Also, the abundance of the *Pseudomonadales* order decreased toward the end of the time series, while the contribution of *Flavobacteriales* simultaneously increased (Fig. 2F). The influence of *Archaea* to the 16S ASV composition was minor at both stations and accounted for only 0.1% and 0.4% of the relative abundance in FSS and GSSS, respectively (Data sets S4 and S5).

The average relative abundance of ASVs assigned to chloroplast (a proxy for all photosynthetic microeukaryotes) in 16S data sets was nearly three times higher in FSS than in GSSS, and the temporal pattern was different: the abundance increased toward the end of the time series in FSS, whereas in GSSS the opposite occurred (Fig. 2E and F).

Environmental variability during the HAB. The surface water properties—temperature and salinity—were relatively similar during the HAB, as observed from both time series stations (FSS and GSSS) at 10-m depth from where microbial biomass was collected (Table S4). The overlying surface water was more stratified in FSS than GSSS. This was due to a low-salinity layer (<30 PSU) which persisted near the surface during the entire time series simultaneously with a strong increase in observed temperature (Fig. S1 and S2). The mixed-layer depth was observed near the surface (3 m) throughout the study period in FSS and in the beginning in the GSSS time series; it then sank to 7 m by the end of the GSSS time series, while the surface water became more homogeneous after day 8 (Fig. S1 and S2). The mean NO_3^- plus NO_2^- concentration was significantly higher in GSSS than in FSS (0.43 and 0.18 μmol L^{-1}, respectively; Tukey test, $P < 0.02$), whereas the $Si(OH)_4$ and PO_4^{3-} concentrations did not show statistically significant differences between stations (Table S4).

Beta diversity in context with the environment. Both the microeukaryotic and prokaryotic components of the HAB-associated microbiome were dissimilar between GSSS and FSS stations, and these communities changed across the time series as inferred from PERMANOVA analysis (see results above in "Microbiome Dynamics across the Bloom"). The beta diversity was measured via unweighted UniFrac distances that were ordinated by distance-based redundancy analysis (dbRDA) to infer the correlation between selected environmental measurements to differences in community composition (Fig. 3). Results of beta diversity analysis in context with environmental factors also corroborated the observed change in community structure during the middle of the time series that was seen and noted above by inspecting changes in relative taxonomic abundance in Fig. 2. The dbRDA analysis (i.e., sum of RDA1 and RDA2) showed that 77.9% and 83.7% of the total variation in the prokaryotic and microeukaryotic community composition were correlated to environmental measurements during the time series (Fig. 3). Most of this variation was explained by the first RDA component (RDA1: 16S, 60.8%; 18S, 72.6%), inferring that the variation of both prokaryotic and microeukaryotic communities between FSS and GSSS may be driven by responses to environmental factors such as mixed-layer depth (MLD), salinity, and NO_3^- plus NO_2^- (Fig. 3), whereas the temporal variability within stations was mainly explained by the second RDA component (RDA2), which accounted for 17.1% and 11.1% of the variance in prokaryotic and microeukaryotic communities, respectively.

Temporal trends and coblooming taxa. The marine microbiome at the two time series stations, FSS and GSSS, was complex and consisted of a minimum of 235 and 161 16S and 18S ASVs, respectively, each maintaining its own dynamic trajectory during the observed time series. Examination and subsequent clustering of the predominant blooming patterns was performed via the k-medoid clustering method. The

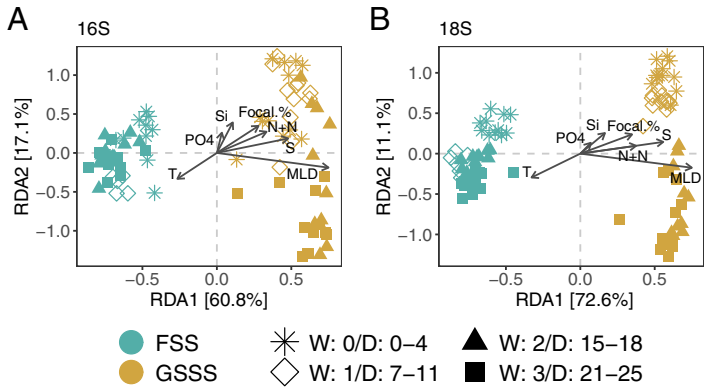

FIG 3 Dissimilarity in prokaryotic and microeukaryotic community composition between sample stations was inferred via beta diversity as measured with unweighted UniFrac distances and related to environmental measurements. (A and B) Distance-based redundancy analysis (dbRDA) biplot of (A) prokaryotes and (B) microeukaryotes. Color represents station and shape represents sample (sample scores) within each sample week. Note that the first sample week is "W: 0". Arrows indicate environmental factors and point to the direction of maximum variation of the respective factor. T, temperature; S, salinity; MLD, mixed-layer depth, Si, $Si(OH)_4$; PO4, PO_4^{3-}; N+N, NO_2^- plus NO_3^-; focal %, relative abundance of the *C. leadbeateri* focal taxon in the 18S data set.

resulting number of clusters per data set and time series station, as assessed via the Calinski-Harabasz index (normalized ratio for inter- and intracluster variance) (Fig. S5), was 3, except for 18S at FSS, where 4 clusters were selected. The temporal pattern of each cluster was specified by its medoid ASV as a representative shape for the cluster's blooming dynamics of microeukaryotes (Fig. 4A and B) and coblooming taxa assigned to 16S ASVs (Fig. 5A and B). The Z-score indicates the magnitude of change (i.e., standard deviations) in relative abundance of each ASV in relation to the mean abundance across time series.

The medoid 18S ASV of clusters 1 and 3, from both stations, exhibited approximately inverse blooming patterns. These clusters also showed strong fluctuation in relative abundances across the time series, including a strong positive and negative shift, respectively, around the middle time points (Fig. 4A and B), whereas the medoid taxon of clusters 2 and 4 in FSS and cluster 2 in GSSS exhibited a short increase in abundance in the beginning or end of the time series (Fig. 4A and B). At both stations cluster 1 and cluster 3 revealed mainly positive and negative correlations to environmental measurements, respectively, although these were not statistically significant (Fig. 4C and D).

The focal ASV belonged to cluster 3 at both stations (Fig. 4A and B). There were several classes of microalgae that cobloomed with the focal ASV, but these were distinct between the FSS and GSSS stations (Fig. 4E and F). In FSS the focal ASV cobloomed with the genera *Teleaulax* (class *Cryptophyceae*) and *Leptocylindrus* (class *Coscinodiscophytina*), which comprised 16 to 53% and 1 to 53% of the relative abundance within their respective cluster 3 (Fig. 4E and genus level abundances of cluster 3 in FSS Data set S6). A diverse composition of ASVs indicative of MAST clades (marine stramenopiles) were also detected, although their relative abundances were minor (<1% of relative abundance within cluster 3). This group was represented by other nano- and picoplankton such as the genera *Telonema* (class *Insertae Sedis*) and *Picomonas* (class *Picomonadida*), the taxa in cluster 1 with an inverse blooming pattern to cluster 3 (Fig. 4C and E and Data set S6). ASVs from the genus *Phaeocystis* predominantly cobloomed at GSSS with the focal ASV (within cluster 3) together with a less abundant group of ciliates (class *Intramacronucleata*) and members belonging to genus *Thalassiosira* (class *Mediophyceae*) (Fig. 4D and F and genus level abundances of cluster 3 in GSSS in Data set S7). ASVs belonging to the class *Dinophyceae* were also included in cluster 3 from GSSS (along with the focal ASV), and these were composed mainly of members classified within the genus *Gymnodinium*.

The blooming patterns of 16S ASVs were also clustered. Among these, two clusters (1 and 2 from FSS and GSSS, respectively) showed significant positive correlation (FSS:

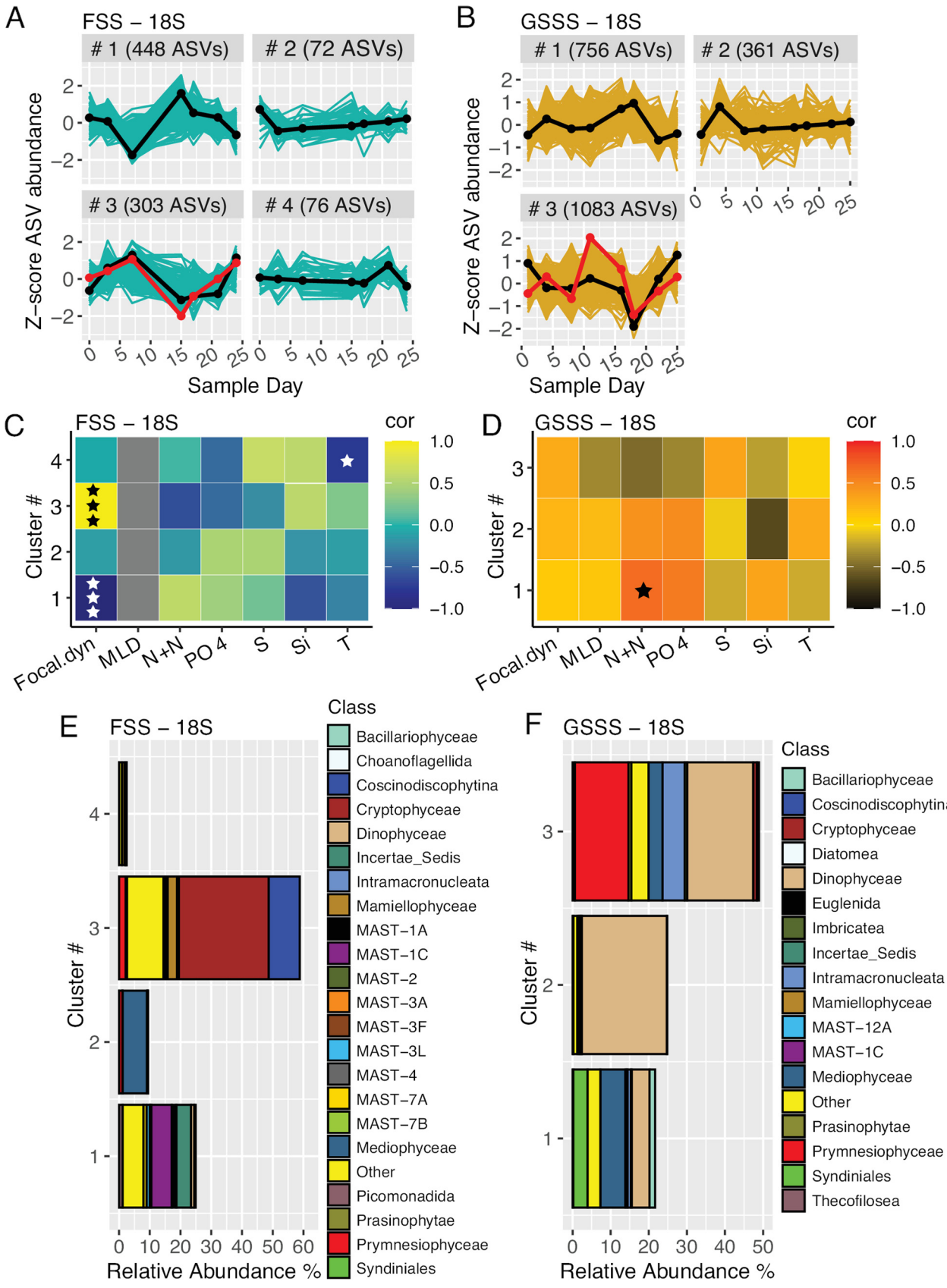

FIG 4 Characterization of major blooming patterns in microeukaryotic communities assessed by k-medoid clustering analysis with Z-transformation and detrending of 18S ASVs. (A and B) Temporal dynamics of microeukaryotic taxa and number of ASVs per defined cluster (A) in FSS and (B) in the

(Continued on next page)

$r = 0.79$, $P = 0.036$ and GSSS: $r = 0.71$, $P = 0.047$) with the focal ASV. Only cluster 2 from station FSS showed a significant negative correlation with the focal ASV ($r = -0.96$, $P < 0.001$) (Fig. 5C and D). The temporal trend represented by the medoid ASV was nearly identical in cluster 3 at both stations, corresponding to the blooming pattern of cluster 2 and inverse blooming pattern of cluster 4 for microeukaryotes in GSSS and FSS, respectively.

We infer that the bacterial taxa from the GSSS station belonging to cluster 2 cobloomed with phototrophic protists in general, because the ASVs assigned to chloroplasts occupied the same cluster (Fig. 5F and 4F). This cluster was also the only one to show a statistically significant correlation with phosphate concentrations (Fig. 5D). The same pattern was not observed in FSS, where approximately two-thirds of chloroplast ASVs were identified within cluster 2 and the rest in cluster 3 (Fig. 5E).

Pearson correlation enabled us to infer that different bacterial communities cobloomed with the *C. leadbeateri* focal taxon, corresponding to the observations within 18S microeukaryotes (Fig. 5C and D). Cluster 1 at station FSS was dominated by the order *Flavobacteriales* (35 to 63% relative abundance within cluster 1) (Fig. 5E) and was dominated by sequences identified within the NS5 marine group but also *Ulvibacter* (genus level abundances of cluster 1 in FSS in Data set S8). ASVs assigned to *Rhodobacterales*, notably the evenly dominating genera *Amylibacter* and *Planktomarina*, also shared similar temporal dynamics with the focal ASV (Fig. 5E and Data set S8). The positive coblooming trend between *Flavobacteriales* and *Rhodobacterales* classes and the focal ASV were not observed at station GSSS.

DISCUSSION

The results from this study show distinct spatial variation and differences in the dynamic microbiome community composition across the portion of the northern Norwegian coast that was strongly affected during the 2019 *Chrysochromulina leadbeateri* HAB. This was a major and disruptive event due to severe fish mortality, and hence there were several sampling campaigns launched simultaneously by public and private stakeholders. Our current study did not capture the onset of the HAB, and to our knowledge, neither did any of the concurrent studies performed by other parties. This is because HAB events such as this are currently impossible to predict. The aim of this molecular-based investigation of the holistic microbiome during the 2019 HAB was to set the blooming pattern of *C. leadbeateri* within the ecological context of its cooccurring community members. Therefore, these results from our amplicon-based sequencing approach are expected to be more complex and distinct from previous, related events that have been characterized by mainly morphology-based taxonomy and cell-counting surveys.

Indication of separate focal blooms. The 2019 HAB was reported on and monitored daily with a focus on afflicted fish farm localities by the Norwegian Directorate of Fisheries (6). According to the prevailing consensus based on reported fish mortality, the toxic bloom of the focal taxon initiated in Ofotfjord (Fig. 1A). The last report on fish mortality in Ofotfjord was dated 4 days before the sample in Ballangen was taken (6); thus, there was, presumably, a mismatch between the bloom peak and time of sampling. We do not have data that represent the community composition during the first reports of fish mortality. This may explain why we found a surprisingly high disparity between expected (i.e., high focal taxon abundance) and observed microbial community composition at Ballangen, which did not correspond with any other sampled microbial community composition (Fig. 1B and C). The microeukaryotic community was

FIG 4 Legend (Continued)
GSSS station. The blooming pattern of each cluster is specified by medoid taxon and drawn with a black line. The red line specifies the blooming pattern of the focal ASV. The *y* axis is the Z-score, indicating a magnitude of change in standard deviations; a value of 0 denotes the mean abundance. (C and D) Heatmap of Pearson's correlation between temporal dynamics of the medoid taxon (Z-scores) of each cluster and the focal ASV (Z-scores) and environmental factors (C) in FSS and (D) in GSSS. Color indicates Pearson's correlation coefficient, and the degree of significance is marked with stars. (one star, $P \leq 0.1$; two stars, $P \leq 0.05$; three stars, $P \leq 0.001$). The gray color for MLD in FSS denotes an undefined correlation, as MLD values remained the same through the study period. Focal.dyn, temporal dynamic of focal ASV; MLD, mixed-layer depth; N+N, NO_2^- plus NO_3^-; PO4, PO_4^{3-}; S, salinity; Si, $Si(OH)_4$; T, temperature. (E and F) Taxonomic profile of the most common microeukaryotes of each cluster as relative abundance in a whole community classified at the class taxonomic rank level in (E) FSS and (F) GSSS.

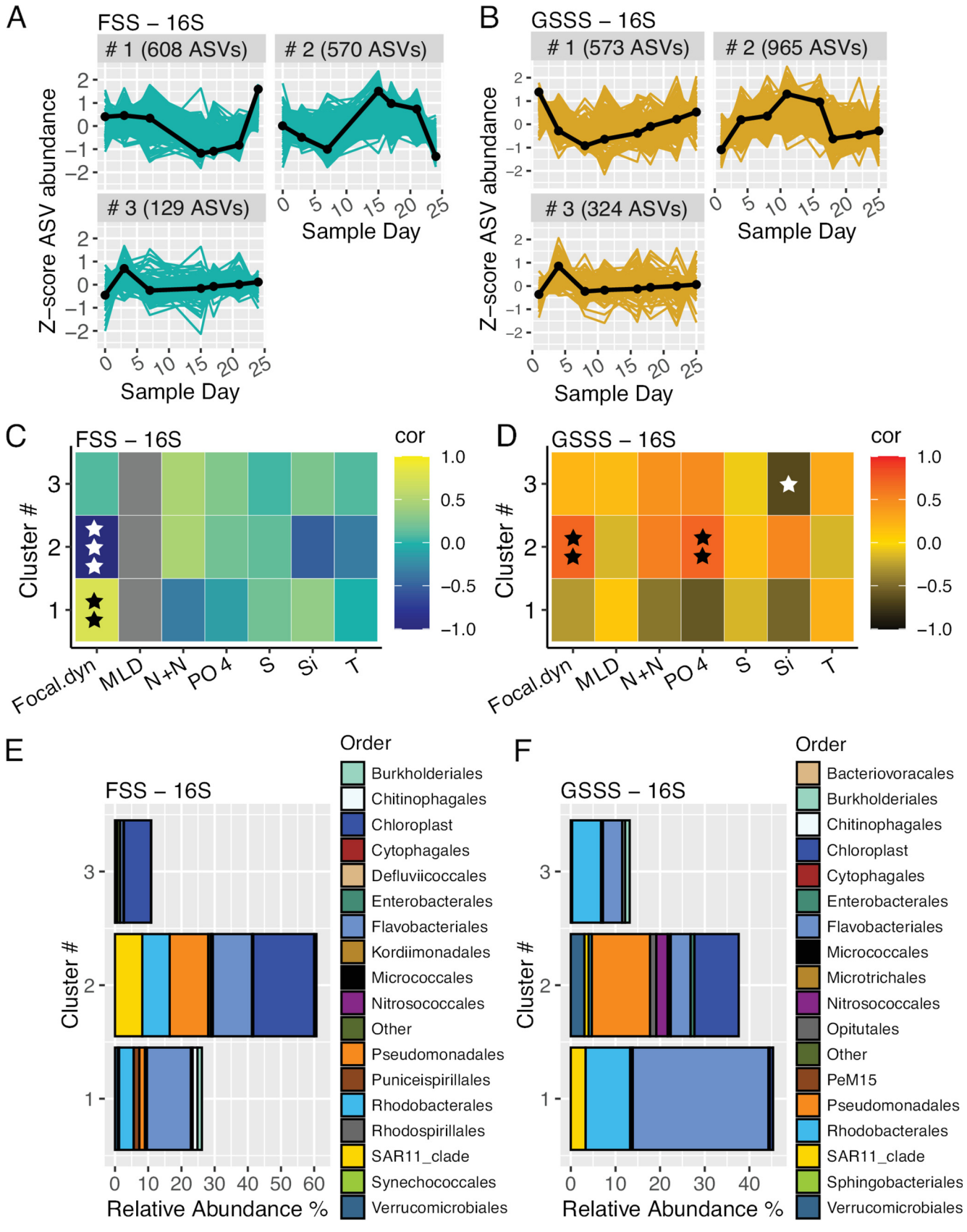

FIG 5 Characterization of major blooming patterns in prokaryotic communities assessed by k-medoid clustering analysis with Z-transformation and detrending of 16S ASVs. (A and B) Temporal dynamics of microeukaryotic taxa and number of ASVs per defined cluster (A) in FSS and (B) in the GSSS

(Continued on next page)

dominated by diatoms, nearly exclusively composed by *Skeletonema*. A similar shift from the presence to absence of *C. leadbeateri* with concurrent predominance of diatoms was observed during the 1991 HAB around Ofotfjord and surrounding areas (23, 24). Correspondingly, the sampled prokaryotic community composition in Ballangen does not presumably represent the situation with *C. leadbeateri* as a disruptive causative agent, as several genera belonging to the observed predominant bacterial order *Alteromonadales* have been found to associate with *Skeletonema* spp. (25).

The focal taxon *C. leadbeateri* is a common and natural member of phytoplankton community along the entire northern Norwegian coast, although its spatial and interannual variation has not been well described, as only two years of monitoring were conducted in the area south and north of Ofotfjord after the 1991 HAB (23, 26). This and the parallel studies provide evidence for high spatial variation in the abundance of the *C. leadbeateri* focal taxon (6, 22). Our results based on relative abundances within 18S rRNA amplicon sequencing data share some reassuring similarities to the reported microscopy cell counts (4, 6) but also 18S amplicon sequence reads presented in another study conducted by John et al. (22) indicating that high *C. leadbeateri* focal taxon abundance occurred in Balsfjord. Thus, this raises the question of whether a bloom of the focal taxon commenced locally in Balsfjord. Due to limited connectivity, it is likely that *C. leadbeateri* blooms developed independently in both fjords since its relative abundance was low in the FSS station (Fig. 2C) and no afflicted fish farms were reported near the FSS station, despite of the affect on fish farms in the area north of Ofotfjord (6). Interestingly, despite high abundance of the focal taxon and effective advection-driven dispersal of cells from the inner part of Balsfjord toward the GSSS and Tussøya stations, only one fish farm near Tussøya was afflicted (Fig. 1A). However, this farm experienced limited impacts, and its relation to the HAB remained somewhat questionable (6). This observation also lends some support to the idea that there may have been at least two distinct physiological states between these two *C. leadbeateri* blooms and that only one of them was harmful.

Localized microbial communities. One of the major questions that drove this study was how the marine microbiome composition compared across locations during the HAB time series. The results revealed distinct communities between sample locations, each possessing different predominating bacterial and eukaryotic microbial groups (Fig. 1 and 2). This observation of spatial heterogeneity provides new information on the development of the late bloom phase within an interconnected coastal area (27). GSSS was the only station where *Phaeocystis* abundance exceeded that of the focal taxon. In fact, the relative abundance of *Phaeocystis* was less than 1% at all other stations, which was an unexpected result given previously reported ubiquity and prolonged prevalence (March to August) in this region (14, 16).

Although the predominant microalgae groups found in the two time series stations were different (FSS: cryptophytes, *Leptocylindrus*, heterotrophic nanoflagellates; GSSS: dinoflagellates, prymnesiophyte, *Thalassiosira*), the most abundant bacterial taxa, i.e., orders *Flavobacteriales*, *Rhodobacterales*, and *Pseudomonadales*, were essentially consistent. Previously reported studies have also shown that members belonging to these orders commonly accompany microalgae in marine environments, except in the case of *Teleaulax* spp. And *C. leadbeateri*, which may be due to the lack of previous records from events such as the 1991 HAB of northern Norway (13, 28–30). The bacterial community compositions obtained from Middle-Balsfjord and South-Tromsø stations were distinct and corresponded to the highest observed relative abundance of the focal

FIG 5 Legend (Continued)

station. The blooming pattern of each cluster is specified by medoid taxon and drawn with a black line. The *y* axis is a Z-score indicating the magnitude of change in standard deviations, and a value of 0 denotes the mean abundance. (C and D) Heatmap of Pearson's correlation between temporal dynamics of the medoid taxon (Z-scores) of each cluster and focal ASV (Z-scores; Fig. 4A and B) and environmental factors (C) in FSS and (D) in GSSS. Color indicates the Pearson's correlation coefficient, and the degree of significance is marked with stars (one star, $P \leq 0.1$; two stars, $P \leq 0.05$; three stars, $P \leq 0.001$). The gray color for MLD in FSS denotes undefined correlation, as MLD values remained the same through the study period. Focal.dyn, temporal dynamic of focal ASV; MLD, mixed-layer depth; N+N, NO_2^- plus NO_3^-; PO4, PO_4^{3-}; S, salinity; Si, $Si(OH)_4$; T, temperature. (E and F) Taxonomic profile of the most common prokaryotes of each cluster as relative abundance in a whole community classified at the class taxonomic rank level (E) in FSS and (F) in GSSS.

taxon. Specifically, they harbored high relative abundances of SAR11 (mainly clade Ia) and low contributions of *Flavobacteriales*, which is interesting given that SAR11 tends to be negatively correlated with copiotrophic bacterial groups before and after the primary phytoplankton bloom (12, 28). However, the single-time-point stations present a major limitation for interpreting the HAB microbiome, given that the time series stations (FSS and GSSS) showed pronounced temporal variability during the event.

Temporal community dynamics. Another major aim of this study was to identify the temporal patterns of the HAB-associated microbiome and attempt to determine which taxa cobloomed with the focal ASV. We found that most of the microeukaryotic and bacterial taxa either cobloomed or inversely cobloomed with the focal ASV; i.e., the clusters that showed significant positive or negative correlation with the focal ASV also had the highest taxonomic richness (Fig. 4 and 5). There is evidence that the most abundant taxa undergo stronger shifts in their abundance than the rare taxa, which corresponds with our results where the most abundant bacterial orders and microeukaryotic classes were mainly found within the clusters of highest temporal variability (31). However, the high number of taxa in these clusters is somewhat surprising with regard to previous findings of highly coherent communities with well-defined groups of organisms with the potential to interact (11). It is likely that the prescribed temporal (sampling) resolution of this study was too coarse to capture the true frequency of taxonomic turnover, which can be very fast (11, 12). However, when an unpredicted and regionally large (250 km wide) HAB occurs, it poses major logistical challenges to react quickly and access the sample locations with a frequency that would be the most optimal from a biological perspective. The choice of optimal sampling locations is also limited by immediate accessibility to sampling resources, such as suitable watercraft.

The environment. The third major question of this study was related to the abiotic environment and how it may have influenced the microbiome composition and presence of the *C. leadbeateri* focal taxon. The HAB—as inferred from the relative abundance of the focal taxon—was stronger at GSSS than at FSS, yet it occurred concurrently at both stations. The strong decrease in *C. leadbeateri* abundance in the middle of the time series coincided, especially at GSSS, with a change in community composition. However, this was evidenced poorly by environmental factors at both stations. Intriguingly, these results are in accordance with previous findings suggesting lower importance of continuous environmental factors such as temperature, inorganic nutrients, and chlorophyll *a* on a change in community composition after seasonal bloom initiation than biotic interactions (12, 31), whereas, a strong periodical physical force (wind, turbulence) can cause a change of the entire community (11). The measured water column properties did not indicate strong vertical mixing. However, the surface water became somewhat more homogenous after the first week in the time series at GSSS as revealed from conductivity-temperature-depth (CTD) profiles (Fig. S2).

The difference in microeukaryotic composition between the two time series stations may be related to environmental factors as revealed by dbRDA analysis (Fig. 3). The phosphate concentration was low at both stations, and the NO_3^- plus NO_2^- level was low in FSS, which potentially promoted the development of communities of heterotrophic and mixotrophic protists. Several MAST clades (e.g., MAST-1C as dominant in FSS) are known to be bacterivores, and *Teleaulax* has been determined to be mixotrophic, feeding heterotrophically on bacteria, thus relaxing the need for inorganic nutrients (32, 33). It is difficult to draw a link between nutrients and the focal taxon with the current data due to a lack of nutrient measurements from stations with high focal taxon abundance, such as Middle-Balsfjord and South-Tromsø. Despite the nutrient information, a plausible connection would be unlikely, as even a 14-year survey of *Chrysochromulina* spp. cell and nutrient concentration in southern Norway did not provide a clear connection (34). However, there are indications that *Chrysochromulina* spp. thrive in high N:P ratios under low-phosphate concentrations, which potentially promote toxicity if the conditions becomes phosphate-limited (34, 35).

Conclusion. A summary of investigations of the 1991 *Chrysochromulina leadbeateri*-related harmful algal bloom in northern Norway shows that it would not have been

possible to predict such an incident, but it would be necessary to launch a coastal monitoring program (3). Three decades later, we fully agree with the latter statement. We certainly have a long way to go in order to predict how ecological principles underpin this sporadic event in a highly variable coastal area, and it is difficult to get there by performing investigations that simply react to only those blooms that have acute economic impacts. It is also difficult to plan to observe such a bloom that happens so infrequently. It has become highly evident that this type of reoccurring bloom is extremely destructive because it causes substantial losses for fish farmers. In 1991 the fish kill damage linked to *C. leadbeateri* was 742 metric tonnes with a corresponding direct short-term economic cost of 3.5 million USD, while in 2019 these values increased to 14,500 tonnes and more than 100 million USD (2). Thus, it is expected that these numbers will become even higher in the future with increasing aquaculture industry, and there is no reason to believe that this type of HAB will not reoccur. It is challenging to draw any conclusions about exact causation behind the 2019 HAB, especially since the natural bloom cycles of *C. leadbeateri* are not well understood. Therefore, this study relying on molecular-based methods provides a first insight on the spatial and temporal variability of the *C. leadbeateri* focal taxon together with its associated marine microbiome. It also supports future molecular-based studies by providing a genetic link with currently available taxonomic annotation between current and 1991 *C. leadbeateri*. Otherwise, the *C. leadbeateri* focal taxon may be overlooked due to database limitations—an issue also present in this study. We found that most of the taxa, including the most abundant members of the prokaryotes and microeukaryotes and the focal taxon, underwent strong and rapid variability in their succession dynamics. These temporal dynamics were poorly connected to the environmental conditions measured, suggesting that other factors such as biological interactions might drive the late bloom dynamics.

MATERIALS AND METHODS

Study areas. Samples for microbial community analyses were collected from two primary time series stations and from eight single-time point stations. Time series sampling was performed between May 27 (sample day 0) and June 21 (sample day 25) in 2019 (exact dates and locations are in Table S1). The first station, in the vicinity of a fish farm (Lerøy Aurora at Solheim, Norway) was named Grøtsund sampling station (GSSS, 69.80° N, 19.36° E). The second station, named Finnfjord sampling station (FSS, 69.19° N, 18.03° E), is located 60 km south of GSSS, within the same interconnected fjord-sound system (Fig. 1A). These time series stations were chosen because they present historical sample locations (15) and provided long-term access to sampling facilities (vessel: ~5 m polarcirkel and laboratories), whereas, the single-time point stations were chosen to gain a geographical representation of the bloom, given the difficulty of running time series collections across the entire affected region. These stations were located mainly in the fjords—between time series stations in the northern part of the study area and south from the time series stations (Fig. 1A). From the single-time point stations, only information on microbial communities (i.e., no additional environmental data) was collected between May 27 and June 21 (Table S1). The data from these samples are not included within the time series analyses but were used to compare the 2019 HAB affected area via spatial variation in the relative abundance of the focal taxon and associated microbial communities.

Sample collection. Each time series station was visited twice a week, except for station FSS, which was sampled once in the second sampling week (starting the week of May 27, 2019). Temperature and salinity profiles down to 15 to 50 m were recorded with a hand-held X2 electron conductivity-temperature-depth (CTD) instrument (AML Oceanographic, Canada). Water samples for inorganic nutrient analysis and microbial biomass were collected from a fixed sampling depth of 10 m using a 1.7-L Niskin bottle to get approximately 8.5 L of seawater. The collected seawater was prefiltered for large particles with a 150-μm plankton mesh and transported to shore in a 15-L Nalgene plastic carboy. All sampling equipment was rinsed with 2% bleach prior to and between each sampling effort, followed by rinsing with MilliQ water and a minimum of two volumes of station sampling water prior to collection. Water samples for macronutrients, silicate [$Si(OH)_4$], phosphate (PO_4^{3-}), and nitrate plus nitrite (NO_3^- plus NO_2^-), were filtered through 47-mm GF/F glass microfiber filters with a pore size of 0.7 mm (Whatman) into 50-mL Falcon tubes using disposable syringes and stored at −20°C (36). Microbial biomass from both the time series and single-time point stations was collected by vacuum filtration onto 0.22-μm polycarbonate filters (Whatman 47-mm Nuclepore polycarbonate track etched membranes; GE Healthcare 111106). All filtering was done inside a sterile laminar flow hood, and the filtered volume per biological replicate ($n = 6$ for time series samples and $n = 6$ or $n = 3$ for single-time point samples) varied between 500 and 750 mL. Filters were immediately flash frozen and stored at −80°C. The DNA extraction and downstream analysis on all the collected (frozen) microbial biomass were performed at the UiT–The Arctic University of Norway as described below.

Environmental factors. The vertical surface water properties from the time series sampling stations (FSS and GSSS) were inspected using CTD profile data (Fig. S1 and S2). The difference in surface water stratification between sampling stations was determined by calculating the mixed-layer depth (MLD) from each CTD profile datum using potential density. A depth of 1 m was used as a reference depth, as the deployed handheld CTD sensor enables measurements near the surface. A density threshold of 0.1 kg m^{-3} was used to define MLD, i.e., the depth below 1 m where the density first exceeds the defined threshold (37). Temperature and salinity values from the depth of 10 m (corresponding to the depth of collected biomass) and MLD values were further used in statistical analyses. As the CTD casts between sampling days 11 and 17 were unsuccessful, temperature, salinity, and MLD values for these days were interpolated using the R function na.approx from the R package zoo v1.8-9 (38) to fill in the missing values. This generated a source of uncertainty and thus may impact our further inferences on the relationship between these parameters and temporal abundance patterns of microbial communities. Nutrient concentrations were analyzed 20 months later at the UiT–The Arctic University of Norway with a Quatro39 autoanalyzer (Seal Analytical, UK) in subsample triplicates. PO_4^{3-} concentrations below the detection limit of 0.04 μmol L^{-1} were replaced with a small value (0.001) to enable the estimation of this variable in statistical analyses.

Unialgal control cultures. *Chrysochromulina leadbeateri* has been identified as a focal taxon of a toxic bloom in 1991 from an isolate that was collected from Vestfjorden, northern Norway (39). This isolate is currently found in the Norwegian Culture Collection of Algae (NORCCA) repository as *Chrysochromulina leadbeateri* UiO-035 (40). Taxonomic identification of the isolate has been mainly based on scale morphology in comparison to holotype (41) and other previous reports on *C. leadbeateri*-like cells both from the Northern and Southern Hemisphere (39). Several *Chrysochromulina* species are characterized by species-specific bilayer scales which have been considered a morphotype-specific characteristic (39). The near-full-length 18S small-subunit (SSU) rRNA gene of *C. leadbeateri* UiO-035 has been sequenced and can be found in GenBank under accession number AM491017. We verified the focal taxon within our field samples by cultivating and sequencing the unialgal *Chrysochromulina leadbeateri* UiO-035 strain as a control at 6°C on f/2 medium (42), fortified with 20 nM selenium. Cells were collected ($n = 6$) and processed identically to the field samples.

Amplicon sequencing. DNA was extracted from filtered samples from the field, and the unialgal control cultures and downstream amplicon sequences were obtained using the protocol described in Aalto et al. (13). All the samples were processed together in accordance with the Earth Microbiome Project protocols (43) with modifications according to Amaral-Zettler et al. (44). This included recommended primers and barcodes for the V4 hypervariable region of the 16S SSU rRNA gene using the V4 forward (515F) and V4 reverse (806R) primers (45), and the V9 hypervariable region of the 18S SSU rRNA was targeted with the V9 forward (1391F) and V9 reverse (EukBr) primers (44). Biological replicates were sequenced on a MiSeq instrument (Illumina, San Diego, CA, USA) according to Caporaso et al. (46) at Argonne National Laboratory (Lemont, IL, USA). The realized length of the merged forward and reverse reads for the 18S data set varied between 151 and 282 bp, and for 16S data set the corresponding range was 152 to 289 bp. Within these variations the 50th percentile of the 7-number summary of sequence length was 197 bp for 18S and 253 bp for 16S.

Amplicon analysis. The amplicon analyses were performed with the QIIME2 environment and using QIIME2 plugins as previously described in Aalto et al. (13). Briefly, Illumina forward and reverse reads and the corresponding barcode files were imported and demultiplexed using the Earth Microbiome Project paired-end flag. All reads were filtered, de-replicated, and chimera-checked using all default parameters in DADA2 v2021.2.0 (47). The reads were merged and amplicon sequence variants (ASVs) were determined using DADA2 v2021.2.0. The DADA2 statistic on sequence reads is provided in Data set S1. A 16S and 18S rRNA gene classifier from the SILVA v138.1 database was trained using RESCRIPt (48, 49). The ASVs were classified with the self-trained classifier database (50). It is noted that the major challenge in 16S- and 18S-based taxonomy is its dependency on the taxonomic resolution limitations of the database. We chose to use all classifications given from the SILVA v138.1 database because this is a standardized approach. Manual curation of taxonomic classification except unialgal controls was beyond the scope of this study.

Within the unialgal control cultures, the 18S amplicon analysis assigned four abundant ASVs (Fig. S3A). All four of these ASVs had identical taxonomic assignments within the SILVA v138.1 database: family, *Prymnesiales*; genus, OLI16029; species, unknown. Of these four ASVs assigned as OLI16029, ASV *24a92740c5af4cd5a5ac0db70830fbc0* (here referred to as the focal ASV) was the most abundant and made up 88% of the sequence reads (Fig. S3B). All four of these ASVs were also present among the field samples, with seven additional ASVs assigned as OLI16029. The sequence of the focal ASV was manually searched against NCBI BLAST. The results showed a sequence match of 100% (query cover 91%) with *C. leadbeateri* UiO-035, but also 99.40% identity (query cover 97%) was found with *C. leadbeateri* UiO-393 strain (NORCCA; GenBank accession number ON815372), which was isolated during the 2019 HAB by John et al. (22). The sequence alignment of all ASVs classified as OLI16029 and the *C. leadbeateri* strains UiO-035 and UiO-393 are shown in Fig. S4. These ASVs are referred to here as *C. leadbeateri*.

Statistics, clustering, and correlation. All ASVs not assigned to the expected kingdom (*Archaea* and *Bacteria*) or chloroplasts were removed along with all mitochondrial assignments from the 16S data set. Since this study did not include measurements of chlorophyll *a* to indicate changes in phototrophic phytoplankton abundance, the 16S ASVs identified as chloroplasts were used as an inference. ASVs assigned to *Archaea*, *Bacteria*, *Vertebrata*, and the phyla *Arthropoda*, *Cnidaria*, *Echinodermata*, *Annelida*, *Nematozoa*, *Nemertea*, *Porifera*, *Mollusca*, *Ctenophore*, and *Tunicata* or phyla belonging to macroalgae and land plants or land fungi such as *Bangiales*, *Floridephycidae*, *Ochrophyta*, *Phragmoplastophyta*,

Ascomycota, *Basidiomycota*, and *Myxogastria* were removed from the 18S data set. Additional information on the number of ASVs and sequencing depths before and after removing taxa is provided in Table S2. The total numbers of classified ASVs in FSS for the 18S and 16S data sets were 900 and 1,309, respectively, and in GSSS there were 2,196 and 1,865, respectively. As an exception regarding the correction of taxonomic annotations, the classified 16S order *Enterobacterales* was manually changed to the closely related order *Alteromondales*, as the main genera of this order were *Pseudoalteromonas*, *Colwellia*, and *Glaciecola*, which are known to be members of the *Alteromonadales* (51).

Downstream analysis was completed in R (52), using the microeco v0.11.0 (53) and vegan v2.5-7 packages (54). This study also used the k-medoid clustering method adapted from a previously described approach applied to time series microbiome data to examine distinct temporal trends in blooming patterns within communities (21). Briefly, ASV counts from each sample type, i.e., sampling station (FSS or GSSS) and PCR amplification primer type (16S or 18S), were preprocessed via Z-score- and variance-stabilizing transformations using the DESeq2 v1.34.0 package in R (55). Pairwise distance matrices were calculated by the Euclidean distance prior to partitioning each sample-specific ASV into k-medoid clusters according to a similarity criterion over the time series. The quality of each cluster per each sample type was assessed via the Calinski-Harabasz index (Fig. S5) (56). Pearson's correlation was used to examine the relationship between each temporal dynamic, represented by medoid ASV (cluster centroids), and environmental measurements but also to obtain the positively and negatively coblooming microalgae and bacterial taxa with focal ASVs.

The difference in microbial communities, i.e., beta diversity, between sampling stations was measured using the unweighted UniFrac distance metric, which measures occurrence—presence/absence of ASVs—and phylogenetic diversity (57). The beta diversity and relationship between community compositions and environmental factors [temperature, salinity, MLD, $Si(OH)_4$, PO_4^{3-}, NO_3^- plus NO_2^-, and relative abundance of the focal taxon (*C. leadbeateri*)] were visualized and conducted via distance-based redundancy analysis (dbRDA). The permutational multivariate analysis of variance (PERMANOVA) was performed to test the (dis)similarity in prokaryotic (*Bacteria* and *Archaea*) and microeukaryotic (phytoplankton and heterotrophic protist) community compositions between stations (pairwise) and within stations (58). The Tukey test was performed on inorganic nutrients and observed number of ASVs to determine if the mean concentration values were statistically different between time series stations (59).

Data repository and reproducible analyses. All sequencing, including raw fastq files and environmental data, is available on the Open Science Framework (osf.io), along with all R Markdown scripts used for analyses and graphing (osf.io/4wjhp/).

SUPPLEMENTAL MATERIAL

Supplemental material is available online only.

SUPPLEMENTAL FILE 1, PDF file, 2 MB.
SUPPLEMENTAL FILE 2, XLSX file, 0.03 MB.
SUPPLEMENTAL FILE 3, XLSX file, 0.1 MB.
SUPPLEMENTAL FILE 4, XLSX file, 0.1 MB.
SUPPLEMENTAL FILE 5, XLSX file, 0.2 MB.
SUPPLEMENTAL FILE 6, XLSX file, 0.2 MB.
SUPPLEMENTAL FILE 7, XLSX file, 0.1 MB.
SUPPLEMENTAL FILE 8, XLSX file, 0.1 MB.
SUPPLEMENTAL FILE 9, XLSX file, 0.1 MB.

ACKNOWLEDGMENTS

We greatly appreciate the logistical support by the staff at Lerøy Aurora's aquaculture facility at Solheim. We also acknowledge the collaboration between Finnfjord AS and UiT-The Arctic University of Norway for lending sampling infrastructure and support. We thank Åge Mohus and Vigdis Tverberg at Nord University for their help with sample coordination in the southern portion of the HAB-affected area. We kindly acknowledge assistance from the Environmental Sample Preparation and Sequencing Facility in the Biosciences Division of the Argonne National Laboratory.

This study was funded directly by the Faculty of Biosciences, Fisheries, and Economics at UiT–The Arctic University of Norway as the "2019 Harmful Algae Rapid Response Plan."

We specifically thank Terje Aspen, Terje Martinussen, and Kathrine Tveiterås for providing rapid support and guidance.

We have no conflicts of interest to declare.

N.J.A. and H.C.B. conceptualized the study. N.J.A., E.G.-M., J.B.S., L.D., C.J.H., and R.A.I. carried out the sampling. N.J.A., H.S., S.K., and S.P. performed lab work and processed amplicon sequence analyses. N.J.A. and H.C.B. conducted data analysis, and N.J.A. wrote the manuscript draft. All authors contributed to the final version.

REFERENCES

1. Hallegraeff GM, Anderson DM, Belin C, Bottein M-YD, Bresnan E, Chinain M, Enevoldsen H, Iwataki M, Karlson B, McKenzie CH, Sunesen I, Pitcher GC, Provoost P, Richardson A, Schweibold L, Tester PA, Trainer VL, Yñiguez AT, Zingone A. 2021. Perceived global increase in algal blooms is attributable to intensified monitoring and emerging bloom impacts. Commun Earth Environ 2:117. https://doi.org/10.1038/s43247-021-00178-8.
2. Karlson B, Andersen P, Arneborg L, Cembella A, Eikrem W, John U, West JJ, Klemm K, Kobos J, Lehtinen S, Lundholm N, Mazur-Marzec H, Naustvoll L, Poelman M, Provoost P, De Rijcke M, Suikkanen S. 2021. Harmful algal blooms and their effects in coastal seas of northern Europe. Harmful Algae 102:101989. https://doi.org/10.1016/j.hal.2021.101989.
3. Rey F. 1991. The Chrysochromulina leadbeateri bloom in Vestfjorden, north Norway, May-June 1991: proceedings from a scientific working meeting. Fisk Hav 3:1–122.
4. Grann-Meyer E. 2020. Chrysochromulina leadbeateri: understanding the presumed causal agent behind the harmful algal bloom of 2019UiT - Arctic University of Norway. https://munin.uit.no/handle/10037/19284?show=full.
5. Statistics Norway. 2020. Aquaculture 2019. https://www.ssb.no/jord-skog-jakt-og-fiskeri/statistikker/fiskeoppdrett. Accessed 23 April 2022.
6. Karlsen KM, Robertsen R, Hersoug B. 2019. Mapping the course of events and preparedness for algal blooms in spring 2019 - Astafjorden, Ofotfjorden, Vestfjorden og Tysfjorden. Nofima AS 29:1–44.
7. Anderson DM, Glibert PM, Burkholder JM. 2002. Harmful algal blooms and eutrophication: nutrient sources, composition, and consequences. Estuaries 25:704–726. https://doi.org/10.1007/BF02804901.
8. Uronen P, Lehtinen S, Legrand C, Kuuppo P, Tamminen T. 2005. Haemolytic activity and allelopathy of the haptophyte Prymnesium parvum in nutrient-limited and balanced growth conditions. Mar Ecol Prog Ser 299:137–148. https://doi.org/10.3354/meps299137.
9. Nielsen TG, Kiørboe T, Bjørnsen PK. 1990. Effects of a Chrysochromulina polylepis subsurface bloom on the planktonic community. Mar Ecol Prog Ser 62:21–35. https://doi.org/10.3354/meps062021.
10. Davidson K, Gowen RJ, Tett P, Bresnan E, Harrison PJ, McKinney A, Milligan S, Mills DK, Silke J, Crooks A-M. 2012. Harmful algal blooms: how strong is the evidence that nutrient ratios and forms influence their occurrence? Estuar Coast Shelf Sci 115:399–413. https://doi.org/10.1016/j.ecss.2012.09.019.
11. Martin-Platero AM, Cleary B, Kauffman K, Preheim SP, McGillicuddy DJ, Alm EJ, Polz MF. 2018. High resolution time series reveals cohesive but short-lived communities in coastal plankton. Nat Commun 9:266. https://doi.org/10.1038/s41467-017-02571-4.
12. Needham DM, Fuhrman JA. 2016. Pronounced daily succession of phytoplankton, archaea and bacteria following a spring bloom. Nat Microbiol 1:16005. https://doi.org/10.1038/nmicrobiol.2016.5.
13. Aalto NJ, Schweitzer H, Krsmanovic S, Campbell K, Bernstein HC. 2022. Diversity and selection of surface marine microbiomes in the Atlantic-influenced Arctic. Front Microbiol 13:892634. https://doi.org/10.3389/fmicb.2022.892634.
14. Degerlund M, Eilertsen HC. 2010. Main species characteristics of phytoplankton spring blooms in NE Atlantic and Arctic waters (68–80° N). Estuaries and Coasts 33:242–269. https://doi.org/10.1007/s12237-009-9167-7.
15. Aalto NJ, Campbell K, Eilertsen HC, Bernstein HC. 2021. Drivers of atmosphere-ocean CO2 flux in northern Norwegian fjords. Front Mar Sci 8. https://doi.org/10.3389/fmars.2021.692093.
16. Eilertsen HC, Falk-Petersen S, Hopkins C, Tande K. 1981. Ecological investigations on the plankton community of Balsfjorden, northern Norway. Sarsia 66:25–34. https://doi.org/10.1080/00364827.1981.10414517.
17. Reigstad M, Wassmann P. 1996. Importance of advection for pelagic-benthic coupling in north Norwegian fjords. Sarsia 80:245–257. https://doi.org/10.1080/00364827.1996.10413599.
18. Eilertsen HC, Taasen J. 1984. Investigations on the plankton community of Balsfjorden, northern Norway. The phytoplankton 1976–1978. Environmental factors, dynamics of growth, and primary production. Sarsia 69:1–15. https://doi.org/10.1080/00364827.1984.10420584.
19. Eilertsen HC, Frantzen S. 2007. Phytoplankton from two sub-Arctic fjords in northern Norway 2002–2004: I. Seasonal variations in chlorophyll a and bloom dynamics. Mar Biol Res 3:319–332. https://doi.org/10.1080/17451000701632877.
20. Fuhrman JA, Cram JA, Needham DM. 2015. Marine microbial community dynamics and their ecological interpretation. Nat Rev Microbiol 13:133–146. https://doi.org/10.1038/nrmicro3417.
21. Coenen AR, Hu SK, Luo E, Muratore D, Weitz JS. 2020. A primer for microbiome time-series analysis. Front Genet 11:310. https://doi.org/10.3389/fgene.2020.00310.
22. John U, Šupraha L, Gran-Stadniczeňko S, Bunse C, Cembella A, Eikrem W, Janouškovec J, Klemm K, Kühne N, Naustvoll L, Voss D, Wohlrab S, Edvardsen B. 2022. Spatial and biological oceanographic insights into the massive fish-killing bloom of the haptophyte Chrysochromulina leadbeateri in northern Norway. Harmful Algae 118:102287. https://doi.org/10.1016/j.hal.2022.102287.
23. Hegseth EN, Eilertsen HC. 1991. The Chrysochromulina leadbeateri bloom in Troms May/June 1991. Development and causes. Fisk Hav 3:45–61.
24. Rey F, Aure J. 1991. The *Chrysochromulina leadbeateri* bloom in the Vestfjord, north Norway, May-June 1991. Environmental conditions and possible causes. Fisk Hav 3:13–32.
25. Deng Z, Chen S, Zhang P, Zhang X, Adams JM, Luo Q, Lin X. 2021. Dynamics of free-living and attached bacterial assemblages in Skeletonema sp. diatom cultures at elevated temperatures. Front Mar Sci 8. https://doi.org/10.3389/fmars.2021.626207.
26. Heidal K, Mohus A. 1995. The toxic Chrysochromulina–salmon disaster of 1991 in northern Norway with some follow-up monitoring records of 1992 and -93, p 163–168. *In* Lassus P, Arzul G, Erard-Le-Denn E, Gentien P, Marcaillou-Le-Baut C (eds), Harmful marine algal blooms. Lavoisier, Paris. France).
27. Wassmann P, Svendsen H, Keck A, Reigstad M. 1996. Selected aspects of the physical oceanography and particle fluxes in fjords of northern Norway. J Mar Syst 8:53–71. https://doi.org/10.1016/0924-7963(95)00037-2.
28. Teeling H, Fuchs BM, Bennke CM, Krüger K, Chafee M, Kappelmann L, Reintjes G, Waldmann J, Quast C, Glöckner FO, Lucas J, Wichels A, Gerdts G, Wiltshire KH, Amann RI. 2016. Recurring patterns in bacterioplankton dynamics during coastal spring algae blooms. Elife 5:e11888. https://doi.org/10.7554/eLife.11888.
29. Ajani PA, Kahlke T, Siboni N, Carney R, Murray SA, Seymour JR. 2018. The microbiome of the cosmopolitan diatom Leptocylindrus reveals significant spatial and temporal variability. Front Microbiol 9:2758. https://doi.org/10.3389/fmicb.2018.02758.
30. Zhou J, Richlen ML, Sehein TR, Kulis DM, Anderson DM, Cai Z. 2018. Microbial community structure and associations during a marine dinoflagellate bloom. Front Microbiol 9:1201. https://doi.org/10.3389/fmicb.2018.01201.
31. Lindh MV, Sjöstedt J, Andersson AF, Baltar F, Hugerth LW, Lundin D, Muthusamy S, Legrand C, Pinhassi J. 2015. Disentangling seasonal bacterioplankton population dynamics by high-frequency sampling. Environ Microbiol 17:2459–2476. https://doi.org/10.1111/1462-2920.12720.
32. Massana R, Terrado R, Forn I, Lovejoy C, Pedrós-Alió C. 2006. Distribution and abundance of uncultured heterotrophic flagellates in the world oceans. Environ Microbiol 8:1515–1522. https://doi.org/10.1111/j.1462-2920.2006.01042.x.
33. Du Yoo Y, Seong KA, Jeong HJ, Yih W, Rho J-R, Nam SW, Kim HS. 2017. Mixotrophy in the marine red-tide cryptophyte Teleaulax amphioxeia and ingestion and grazing impact of cryptophytes on natural populations of bacteria in Korean coastal waters. Harmful Algae 68:105–117. https://doi.org/10.1016/j.hal.2017.07.012.
34. Dahl E, Bagøien E, Edvardsen B, Stenseth NC. 2005. The dynamics of Chrysochromulina species in the Skagerrak in relation to environmental conditions. J Sea Res 54:15–24. https://doi.org/10.1016/j.seares.2005.02.004.
35. Edvardsen B, Imai I. 2006. The ecology of harmful flagellates within Prymnesiophyceae and Raphidophyceae, p 67–79, Ecology of harmful algae. Springer, New York, NY.
36. Strickland JDH, Parsons TR. 1972. A practical handbook of seawater analysis. 2nd edition. Ottawa, Canada, Fisheries Research Board of Canada, 310pp. (Bulletin Fisheries Research Board of Canada, Nr. 167 (2nd ed)). https://doi.org/10.25607/OBP-1791.
37. Peralta-Ferriz C, Woodgate RA. 2015. Seasonal and interannual variability of pan-Arctic surface mixed layer properties from 1979 to 2012 from hydrographic data, and the dominance of stratification for multiyear mixed layer depth shoaling. Prog Oceanogr 134:19–53. https://doi.org/10.1016/j.pocean.2014.12.005.
38. Zeileis A, Grothendieck G. 2005. zoo: S3 infrastructure for regular and irregular time series. arXiv. https://arxiv.org/abs/math/0505527.
39. Eikrem W, Throndsen J. 1998. Morphology of Chrysochromulina leadbeateri (Prymnesiophyceae) from northern Norway. Phycologia 37:292–299. https://doi.org/10.2216/i0031-8884-37-4-292.1.
40. Edvardsen B, Eikrem W, Throndsen J, Saez AG, Probert I, Medlin LK. 2011. Ribosomal DNA phylogenies and a morphological revision provide the

basis for a revised taxonomy of the Prymnesiales (Haptophyta). Eur J Phycol 46:202–228. https://doi.org/10.1080/09670262.2011.594095.
41. Estep K. 1984. Chloroplast containing microflagellates in natural populations of north Atlantic nanoplankton, their identification and distribution; including a description of 5 new species of Chrysochromulina (Prymnesiophyceae). Protistologica 20:613–634.
42. Guillard RR. 1975. Culture of phytoplankton for feeding marine invertebrates, p 29–60. *In* Smith WL, Chanley MH (ed), Culture of marine invertebrate animals. Plenum Press, New York, NY.
43. Gilbert JA, Meyer F, Antonopoulos D, Balaji P, Brown CT, Brown CT, Desai N, Eisen JA, Evers D, Field D, Feng W, Huson D, Jansson J, Knight R, Knight J, Kolker E, Konstantindis K, Kostka J, Kyrpides N, Mackelprang R, McHardy A, Quince C, Raes J, Sczyrba A, Shade A, Stevens R. 2010. Meeting report: the terabase metagenomics workshop and the vision of an Earth microbiome project. Stand Genomic Sci 3:243–248. https://doi.org/10.4056/sigs.1433550.
44. Amaral-Zettler LA, McCliment EA, Ducklow HW, Huse SM. 2009. A method for studying protistan diversity using massively parallel sequencing of V9 hypervariable regions of small-subunit ribosomal RNA genes. PLoS One 4:e6372. https://doi.org/10.1371/journal.pone.0006372.
45. Walters W, Hyde ER, Berg-Lyons D, Ackermann G, Humphrey G, Parada A, Gilbert JA, Jansson JK, Caporaso JG, Fuhrman JA, Apprill A, Knight R. 2016. Improved bacterial 16S rRNA gene (V4 and V4–5) and fungal internal transcribed spacer marker gene primers for microbial community surveys. mSystems 1:e00009-15. https://doi.org/10.1128/mSystems.00009-15.
46. Caporaso JG, Kuczynski J, Stombaugh J, Bittinger K, Bushman FD, Costello EK, Fierer N, Peña AG, Goodrich JK, Gordon JI, Huttley GA, Kelley ST, Knights D, Koenig JE, Ley RE, Lozupone CA, McDonald D, Muegge BD, Pirrung M, Reeder J, Sevinsky JR, Turnbaugh PJ, Walters WA, Widmann J, Yatsunenko T, Zaneveld J, Knight R. 2010. QIIME allows analysis of high-throughput community sequencing data. Nat Methods 7:335–336. https://doi.org/10.1038/nmeth.f.303.
47. Callahan BJ, McMurdie PJ, Rosen MJ, Han AW, Johnson AJA, Holmes SP. 2016. DADA2: high-resolution sample inference from Illumina amplicon data. Nat Methods 13:581–583. https://doi.org/10.1038/nmeth.3869.
48. Quast C, Pruesse E, Yilmaz P, Gerken J, Schweer T, Yarza P, Peplies J, Glöckner FO. 2013. The SILVA ribosomal RNA gene database project: improved data processing and web-based tools. Nucleic Acids Res 41:D590–D596. https://doi.org/10.1093/nar/gks1219.
49. Robeson MS II, O'Rourke DR, Kaehler BD, Ziemski M, Dillon MR, Foster JT, Bokulich NA. 2020. RESCRIPt: Reproducible sequence taxonomy reference database management for the masses. bioRxiv. https://doi.org/10.1101/2020.10.05.326504.
50. Yilmaz P, Parfrey LW, Yarza P, Gerken J, Pruesse E, Quast C, Schweer T, Peplies J, Ludwig W, Glöckner FO. 2014. The SILVA and "all-species living tree project (LTP)" taxonomic frameworks. Nucleic Acids Res 42:D643–D648. https://doi.org/10.1093/nar/gkt1209.
51. Parte AC, Carbasse JS, Meier-Kolthoff JP, Reimer LC, Göker M. 2020. List of Prokaryotic names with Standing in Nomenclature (LPSN) moves to the DSMZ. Int J Syst Evol Microbiol 70:5607–5612. https://doi.org/10.1099/ijsem.0.004332.
52. R Core Team. 2021. R: A language and environment for statistical computing. R Foundation for Statistical Computing, Vienna, Austria.
53. Liu C, Cui Y, Li X, Yao M. 2021. microeco: an R package for data mining in microbial community ecology. FEMS Microbiol Ecol 97:fiaa255. https://doi.org/10.1093/femsec/fiaa255.
54. Oksanen J, Blanchet FG, Kindt R, Legendre P, Minchin PR, O'Hara R, Simpson GL, Solymos P, Stevens MHH, Wagner H. 2013. vegan: community ecology package, version 2. Creative Commons, San Francisco, CA.
55. Love MI, Huber W, Anders S. 2014. Moderated estimation of fold change and dispersion for RNA-seq data with DESeq2. Genome Biol 15:550. https://doi.org/10.1186/s13059-014-0550-8.
56. Lord E, Willems M, Lapointe F-J, Makarenkov V. 2017. Using the stability of objects to determine the number of clusters in datasets. Information Sciences 393:29–46. https://doi.org/10.1016/j.ins.2017.02.010.
57. Lozupone C, Lladser ME, Knights D, Stombaugh J, Knight R. 2011. UniFrac: an effective distance metric for microbial community comparison. ISME J 5:169–172. https://doi.org/10.1038/ismej.2010.133.
58. Anderson MJ. 2001. A new method for non-parametric multivariate analysis of variance. Austral Ecol 26:32–46. https://doi.org/10.1111/j.1442-9993.2001.01070.pp.x.
59. Abdi H, Williams LJ. 2010. Tukey's honestly significant difference (HSD) test. Encyclopedia of Res Design 3:1–5. https://doi.org/10.4135/9781412961288.